Hindawi
Advances in Civil Engineering
Volume 2019, Article ID 7164373, 15 pages
https://doi.org/10.1155/2019/7164373

Research Article

Damage Concentration Effect of Multistory Buckling-Restrained Braced Frames

Hanqin Wang,[1] Yulong Feng,[1] Jing Wu,[2] Qing Jiang,[1] and Xun Chong[1]

[1]*School of Civil Engineering, Hefei University of Technology, Hefei, Anhui 230009, China*
[2]*Key Laboratory of Concrete & Prestressed Concrete Structures, Ministry of Education, Southeast University, Sipailou 2, Nanjing 210096, China*

Correspondence should be addressed to Yulong Feng; feng_yulong@126.com

Received 7 January 2019; Revised 26 February 2019; Accepted 11 March 2019; Published 27 March 2019

Academic Editor: Melina Bosco

Due to the low postyield stiffness of buckling-restrained braces (BRBs), multistory buckling-restrained braced frames (BRBFs) subjected to earthquakes are prone to lateral deformations and damage concentrations at certain stories, which is deemed a damage concentration effect (DCE). A series of nonlinear pushover analyses and response history analyses are conducted to investigate the key factors affecting the DCE of BRBFs. Two comparisons of the DCE are performed for different types of structures and different beam-to-column connections in the main frame (MF). These comparisons show that BRBFs equipped with BRBs as the main earthquake resistance system have a more serious DCE than the traditional moment-resisting frame or conventional braced frame and that the MF stiffness significantly affects the structural residual displacement and DCE. Then, parametric analyses are performed to investigate the influence of two stiffness distribution parameters (in the horizontal and vertical directions) on the DCE of a 6-story BRBF dual system designed according to the Chinese seismic code. The results show that increasing the MF stiffness and avoiding abrupt changes in the BRB stiffness between stories can effectively mitigate the DCE of BRBFs. Finally, the correlations between various damage performance indices are analyzed. A low statistical correlation between the peak and residual drift responses can be observed in BRBFs. Therefore, it is recommended that the DCE be considered in BRBF design.

1. Introduction

A summarized study [1] noted that a buckling-restrained brace (BRB) can prevent buckling under a random seismic force, resulting in excellent ductility and stable hysteretic performance and thereby overcoming the compression buckling shortcoming of conventional steel braces (CBs). In addition, the seismic performance of buckling-restrained braced frames (BRBFs) has been numerically analyzed and verified via experimentation, with the results showing that the added BRBs are effective in dissipating energy and controlling the interstory drift [2–5]. The combination of a BRB and a moment-resisting frame (MRF) as a structural system provides an efficient lateral resistance and energy dissipation capacity and is currently widely used in earthquake engineering [6].

Previous studies [7–9] thoroughly examined the damage concentration effect (DCE) and the soft-story mechanism of conventional steel concentrically braced frames (CBFs) under ground shaking induced by strong earthquakes; these studies considered the overall compression-induced buckling of the braces. However, although the overall buckling of a steel core component is restrained by its external encasing mortar and steel tube, BRBFs are prone to large permanent drifts and damage concentrations at certain stories of a structure because of the low postyield stiffness of BRBs [10, 11]. Fahnestock et al. [12] performed a series of nonlinear response history analyses (NRHAs) and a hybrid test for a 4-story BRBF subjected to two sets of ground motions corresponding to moderate and major earthquakes. The large residual drifts observed indicated one potential drawback of the BRBF system, as these large residual drifts may present significant challenges when seeking to return the system to service after a major seismic event. Erochko et al. [13] compared the residual drift responses of special moment-resisting frames (SMRFs) and BRBFs in steel

buildings designed according to the American seismic code. They noted that the SMRFs and BRBFs had similar peak drifts, but the BRBFs experienced larger residual drifts.

Currently, several approaches have been explored by researchers to mitigate the DCE and to achieve a smaller residual displacement response in structures with BRBs. These approaches can be classified into three categories. The first category comprises methods based on dual systems, where an MRF is used in addition to a BRBF. To reduce the residual story drift, Kiggins and Uang [14] suggested a dual system design in which the addition of backup MRFs can serve as a restoring force mechanism. Ariyaratana and Fahnestock [15] noted that the reserve strength provided by the moment-resisting connections within a BRBF and/or an SMRF, in parallel with the BRBF used to create a dual system configuration, played a critical role in the residual displacement response and soft-story mechanism of BRBFs. Similarly, Ghowsi and Sahoo [16] investigated the effect of beam-column connections on the overall seismic response of a medium-rise BRBF. Sahoo and Chao [17] proposed a stiffness-based design for BRBFs to control the residual interstory drifts by increasing the elastic story stiffness using column sections with a higher moment of inertia, which is essentially a dual system. The second category contains methods based on self-centering systems, which apply the posttensioned prestressed technique to traditional BRBs to form self-centering BRBs (SC-BRB). Miller et al. [18] presented and experimentally investigated a nickel-titanium shape memory alloy (SMA) SC-BRB, where the BRB component provides energy dissipation and the SMA provides self-centering and additional energy dissipation. Zhou et al. [19] developed a dual-tube SC-BRB with basalt fiber-reinforced polymer tendons and verified its hysteric and self-centering performance via an 1840 mm long specimen test. The third category consists of methods based on spine systems. Tremblay [20] proposed a dual steel braced frame achieving a stable inelastic seismic response by replacing some CBs with BRBs in CBFs. Simpson and Mahin [21] investigated the seismic performance of several different strongback spine configurations with BRBs. The experimental results showed that spine systems can effectively reduce the concentration of deformations. Takeuchi et al. [22] proposed a nonuplifting spine frame system with two replaceable BRBs at the bases of the frames to concentrate the major damage into the BRBs and prevent structural collapse. Chen et al. [23] designed a tall steel-braced frame with segmental elastic trussed spines and a uniform story drift response can be found in this newly proposed system.

The dual systems and self-centering systems shown in the above studies essentially provide a postyield stiffness for BRBFs, which has a critical influence on the residual deformation behavior. The spine systems use their very large stiffness to force the structural deformations to be uniform, thus mitigating the DCE. In this paper, two comparisons of the DCE for different structural types and different beam-to-column connections of a frame are made to illustrate the obvious DCE of BRBFs. A 6-story BRBF dual system is then designed according to the Chinese seismic code [24] as a benchmark model. Based on this model, this paper evaluates the influence of two structural parameters characterizing the stiffness distribution, i.e., the BRB-frame stiffness ratio and the BRB stiffness ratio between stories, on the structural DCEs. A series of static nonlinear pushover analyses (NPAs) and NRHAs are then conducted to evaluate the DCE.

2. Description of DCE in BRBFs

2.1. Damage Mechanisms. A structure and its components should have sufficient ductility to avoid brittle failure and improve the structural seismic performance. However, only when structural damage occurs and develops in accordance with an expected pattern, namely, when the structural damage mechanism is designed and controlled, increasing the deformation capability of components is meaningful for improving the structural seismic capacity. Therefore, although BRBs have a large ductility and stable hysteretic energy dissipation capacity, it is necessary to explore the damage mechanisms and DCE of BRBFs. Then, corresponding targeted measures can be taken to avoid the damage concentration mechanism and mitigate the DCE.

The beam-column connections in BRBFs are often designed using simple connections [10–12] that exhibit a weak moment-resisting capacity and can be approximately regarded as pin connections. The columns are often fixed to the foundation at the bottom level. After neglecting the lateral stiffness of the frame columns, the structural seismic force is fully undertaken by the BRBs. Therefore, a BRBF with pin beam-to-column connections is a structure equipped with BRBs as a main lateral resistance system, where the structural reserve strength and postyield stiffness can be neglected. For the BRBF dual system, the yielding and energy dissipation by the BRBs is the first line of defense for protecting the moment-resisting connections within the BRBF or an MRF in parallel with the BRBF, which acts as the second line of defense.

Figure 1 shows the damage mechanisms of BRBFs. The BRB-beam-column damage mechanism, which occurs mainly because the design yield strength of the beam-column members is often greater than that of the BRBs, can be observed in the single-story structures shown in Figures 1(a) and 1(d). For multistory structures, the yield order between different stories significantly affects the damage mechanisms and seismic behavior. The BRBs at all the stories cannot simultaneously enter the yield stage during an earthquake. The yield of the BRBs at one story may cause a dramatic story stiffness difference between the yield story and elastic stories due to the low postyield stiffness of the BRBs, forming a soft story in the BRBFs. Figures 1(b) and 1(e) show a damage concentration mechanism in which the BRBs yield only at a certain story or stories, while the structural members at other stories retain their elastic state. When structures are designed well, the frame undergoes damage after the BRBs yield at all stories, forming a uniform damage mechanism, as shown in Figures 1(c) and 1(d). The BRBFs with rigid beam-column connections have damage mechanisms similar to those with pin beam-column connections, although the additional moment-resisting

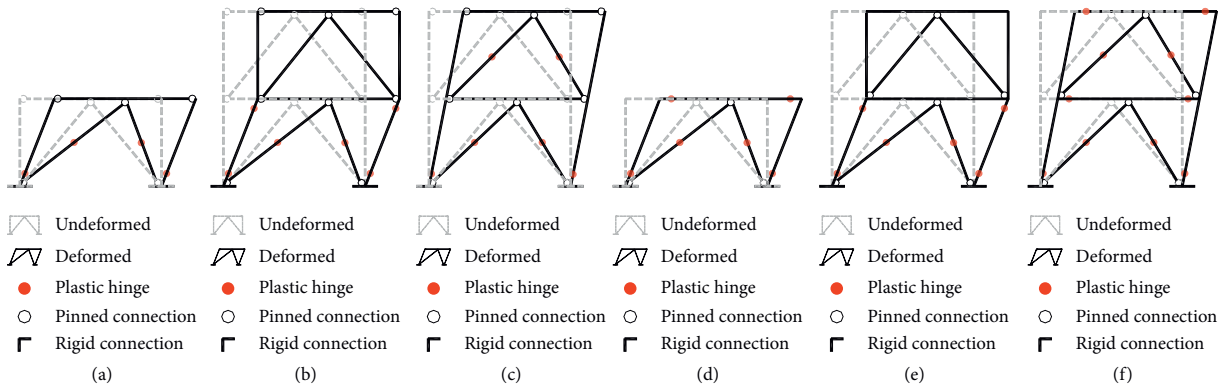

Figure 1: Damage mechanisms of BRBFs with pin and rigid beam-column connections.

connections (dual system) can effectively reduce the residual displacement.

As shown in Figures 1(b) and 1(e), after forming a soft story, the concentration of the deformations in the story can intensify the damage to the BRBs and frame at the story level and amplify the structural P-Delta effects, in turn magnifying the DCE. This significant residual deformation is costly or infeasible to repair. The damage concentration mechanism not only makes it more difficult for the BRBs at the other stories to enter the yield state but may also result in a low cycle fatigue fracture of the BRBs at the soft story after experiencing a considerable repeated strain, causing interstory collapse. In addition, several BRBs, as an energy dissipation device, cannot yield and dissipate earthquake energy under a major earthquake, which is wasteful and unreasonable. Therefore, the DCE of BRBFs and the key factors affecting the DCE are worth investigating.

2.2. Damage Performance Indices. This paper examines the seismic response of six structural damage indices. The maximum interstory drift ratio θ_{max} and roof displacement u_r are often used in the design of a structure to verify whether the structure has enough stiffness to resist a seismic force. MacRae et al. [25] proposed a drift concentration factor (DCF) performance index, which was used to measure the distributions of the structural deformation and seismic energy along the height. The DCF is defined as the ratio of θ_{max} to the average drift ratio θ_{ave}, as shown in equation (1). Note that θ_{max} and θ_{ave} are the maximum and average values of the interstory drift ratios from all structural stories. For an NRHA, the peak interstory drift ratios are used to calculate θ_{max} and θ_{ave}:

$$\mathrm{DCF} = \frac{\theta_{max}}{\theta_{ave}}. \tag{1}$$

Figure 2 shows the calculation process and the result of the upper limit of the DCF for a two-story MRF structure. Figure 2(a) presents the structural elastic deformation and interstory drift ratio, where the story height is the same (h), the lateral force at the first floor (F) is 0.5 times that at the second floor, and k_1 and k_2 are the first and second story stiffnesses, respectively. The DCF of a two-story MRF (DCF_2) is calculated based on equation (1) and Figure 2(a), as shown in equation (2). Figure 2(b) plots the DCF_2-k_1/k_2 curve using equation (2). When k_1/k_2 is less than 1.5, the DCF increases from 1.0 to 2.0 as k_1/k_2 decreases. For the BRBF, k_1/k_2 decreases because of the dramatic story stiffness difference between the yield story and elastic stories, implying that the DCF increases when the BRBF is in the elastoplastic stage.

$$\mathrm{DCF}_2 = \begin{cases} \dfrac{3}{1.5 + (k_1/k_2)}, & k_1/k_2 \le 1.5, \\ \dfrac{2(k_1/k_2)}{1.5 + (k_1/k_2)}, & k_1/k_2 > 1.5. \end{cases} \tag{2}$$

Examining the maximum response, the residual deformation indices, including the residual drift ratio θ_{rmax} and residual roof displacement u_{rr}, are directly related to the cost of repair after an earthquake, which should be less than the cost of rebuilding. McCormick et al. [26] found that when θ_{rmax} exceeds 0.5%, the repair costs exceed the rebuilding costs. The residual drift concentration factor (RDCF) is defined in equation (3), which is similar to equation (1). The DCF and RDCF vary from 1 to the number of stories n.

$$\mathrm{RDCF} = \frac{\theta_{rmax}}{\theta_{rave}}. \tag{3}$$

3. Comparative Analysis of the DCE

3.1. Comparisons among Different Types of Structures. Figure 3(a) shows four types of structures used to illustrate the obvious DCE in BRBFs. The main frame (MF) structure is a 6-story steel MRF with 3 spans; each span is 8 m. The height of the base story is 5 m, and the height of each subsequent story is 4 m. The column section is made of rectangular $400 \times 400 \times 20$ steel tubing (with a width and wall thickness of 400 mm and 20 mm, respectively), and the beam section is made of $450 \times 250 \times 10 \times 16$ H-style steel (with a height, width, web thickness, and flange thickness of 450 mm, 250 mm, 10 mm, and 16 mm, respectively). The equivalent values of the dead load and live load on the beams of each story are 36 kN/m and 12 kN/m, respectively.

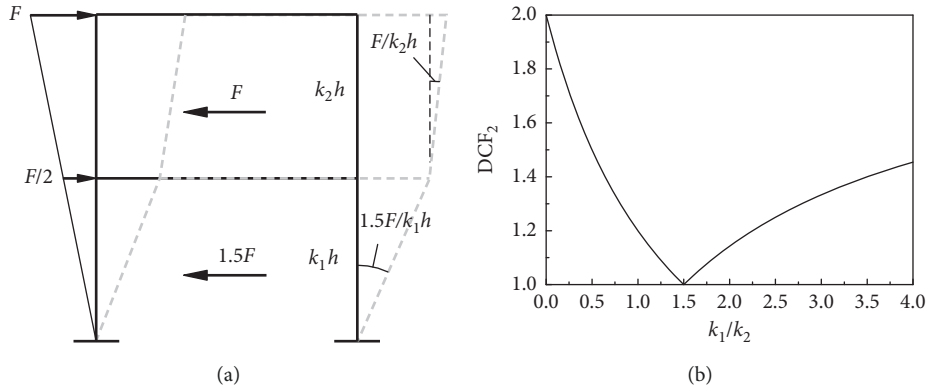

Figure 2: DCF calculation for a two-story MRF: (a) structural deformation and interstory drift ratio; (b) DCF_2-k_1/k_2 curve.

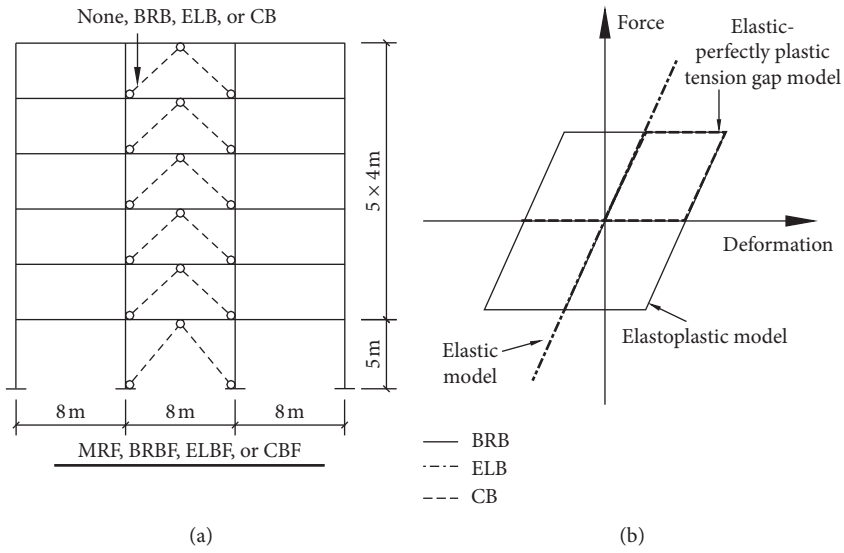

Figure 3: Four types of structures: (a) structural layouts; (b) hysteresis models of braces.

The equivalent mass of each story is 137143 kg. The MF beams and columns are made of Q345-grade steel with a yield strength of 345 MPa. The middle span is arranged using BRBs, elastic steel braces (ELBs), and CBs to build the BRBF, elastic braced frame (ELBF), and CBF, respectively. Note that the brace cannot always remain in the elastic state as the earthquake intensity increases, and the ELBF is used only as an ideal structural model for the comparative analyses. The area of all types of braces is 2700 mm^2, and all braces are made of Q235-grade steel with a yield strength of 235 MPa. The elastic modulus E of all steel members is 2.06×10^{11} N/m^2.

OpenSees [27] numerical simulation software is used for the structural analysis, including modal analyses, NPAs, and NRHAs. The nonlinear analysis considers the P-Delta effects. An inverted triangle lateral force distribution is applied to the structure during the entire NPA process. Tangent stiffness proportional Rayleigh damping is used for the NRHAs, with an intrinsic damping ratio of 0.05 assumed in the first and second modes. The columns and beams are modeled using nonlinear beam-column elements in a bilinear model with a postyield stiffness ratio of 0.01. The BRB and ELB are simulated using truss elements with an ideal elastoplastic model and elastic model, respectively. Figure 3(b) shows the hysteresis responses of the BRB, ELB, and CB. Note that fiber beam-column element models with initial imperfections are often used to simulate the buckling behavior of the CB in many previous studies [28, 29]. For simplicity, the CB in this paper is roughly built using a truss element with an elastic-perfectly plastic tension gap model, where the stress-strain relationship is the ideal elastoplastic model in the tension stage and the stress is equal to zero in the compression stage. An accurate numerical model of the braces and frame members should be considered in further study of the structural damage concentration.

The north-south component of the motion recorded in El Centro during the Imperial Valley, California, earthquake of May 18, 1940 [30], is selected, and its peak acceleration is set to 4 m/s^2 for the NRHA (El-Centro-4), as shown in Figure 4. The fundamental periods of structures with and without braces are 0.86 s and 1.76 s, respectively. The displacement responses of the MRF, BRBF, ELBF, and CBF are

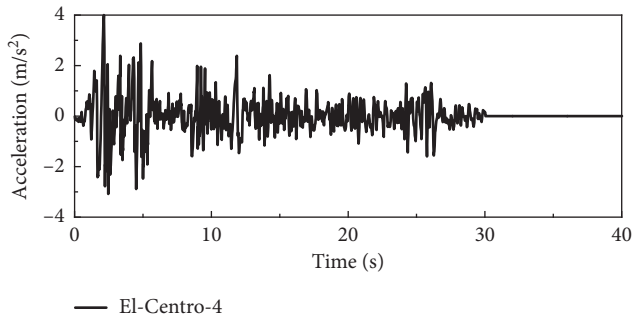

Figure 4: Time-history acceleration of El-Centro-4.

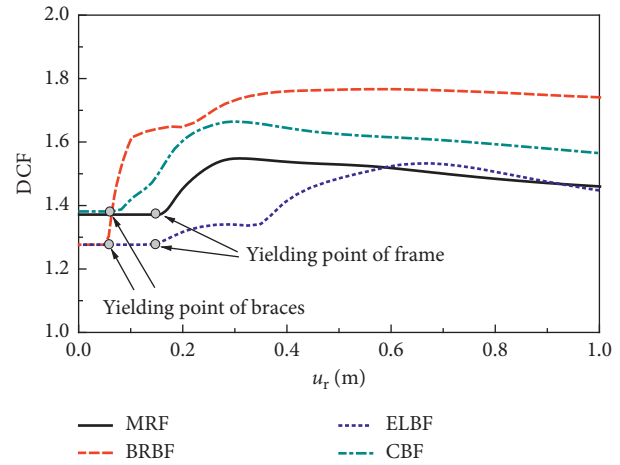

Figure 5: DCF responses of four types of structures.

0.193 m, 0.095 m, 0.176 m, and 0.139 m, respectively. The MRF fundamental period is the largest, and its lateral stiffness is the smallest, which leads to a large displacement response. The CBF has a larger displacement response because the buckling of the CBs can lead to a sudden decrease in the structural stiffness. The displacement response of the ELBF is greater than that of the BRBF, which indicates that the yielding of the BRBs can dissipate seismic energy and reduce the structural displacement.

Figure 5 compares the DCF responses of the MRF, BRBF, ELBF, and CBF subjected to a NPA. As shown, the DCF response of the BRBF is notably greater than that of the other structures after the roof displacement approximately reaches 0.1 m. When the interstory shear forces are given, the structural DCF is directly determined by the relative stiffness between different stories. The stiffness distribution changes as the members in the structure yield, thus changing the structural DCF. The yield roof displacements of the braces and MF are approximately 0.06 m and 0.15 m, respectively, and the corresponding yield roof drift ratios are 1/420 and 1/170, respectively. The DCF*s* of the BRBF and CBF greatly increase due to the braces yielding at one story or certain stories, while those of the MRF and ELBF change slightly due to the yielding of the frame beams and columns. The structural DCF tends to be constant when u_r is large, implying that the whole structure yields and the structural damage mechanism is completely formed. It is difficult for a new member to yield, and the structure cannot continually bear the horizontal load. After the braces at a certain story yield, the difference in the interstory stiffness between the yield and elastic stories is the equivalent interstory stiffness provided by two braces in the BRBF and one brace in the CBF (due to the earlier buckling of the CBs). Therefore, the BRBF is shown to have a more significant DCE than the MRF or CBF, although the BRB has a more stable hysteretic performance than the other types of braces.

When the roof displacement reaches 0.5 m, the maximum vertical deformation at the beam midlength in the CBF occurs on the second story and reaches 0.096 m (down), while that in the BRBF is almost equal to zero. The results show that the beams in the CBF need to bear a larger vertical unbalanced force after the buckling of the CB in compression than the BRBF. A detailed study on the influence of the beam flexural stiffness on the seismic response of steel chevron CBFs can be found in D'Aniello et al. [31].

3.2. Comparisons among Different Beam-To-Column Connections of the Frame. Previous studies [12, 32, 33] found that the seismic performance of braced frames was significantly influenced by the type of beam-to-column connections. Costanzo et al. [32] noted that rigid beam-to-column connections can have beneficial effects, providing an additional reserve of strength and stiffness for chevron CBFs. Fahnestock et al. [12] and Wigle and Fahnestock [33] conducted large-scale experimental and numerical studies of BRBFs, respectively. The results showed that the connection configurations have a significant impact on the global system response and localized connection demands. Furthermore, the full ductility capacity of the BRBs cannot be realized due to an early-age connection failure.

Three contrasting models are constructed, as shown in Figure 6, to analyze the influence of the MF beam-to-column connections on the seismic performance and damage mechanisms of the BRBFs. Figure 6(a) shows the BRBF with rigid beam-to-column connections (BRBF-RBC), which is the same model as presented in Section 3.1. The model shown in Figure 4(b) is a BRBF with pin beam-to-column connections (BRBF-PBC) based on the BRBF-RBC. The column constraint at the floor level is released to form a BRB truss (BRBT) system (See Figure 6(b)), and its interstory stiffness is provided only by the BRBs.

Figure 7 compares the roof displacement time-history responses of the three models under the effect of El-Centro-4. The peak roof displacements of the BRBF-RBC, BRBF-PBC, and BRBT are 0.095 m, 0.135 m, and 0.156 m, respectively, and their residual roof displacements are 0.002 m, 0.036 m, and 0.120 m, respectively. The residual displacements are mainly contributed by the BRBs, and the ratio between the residual and peak roof displacements is 2%, 27%, and 77%, respectively. These results are mainly due to the small MF elastic stiffness in the BRBF-PBC and BRBT, implying that the MF stiffness is helpful for reducing the residual displacement of the BRBFs.

Figure 8 plots the interstory displacement time-history curves at each floor of the BRBT model under the effect of El-Centro-4. It can be observed that the displacements of all

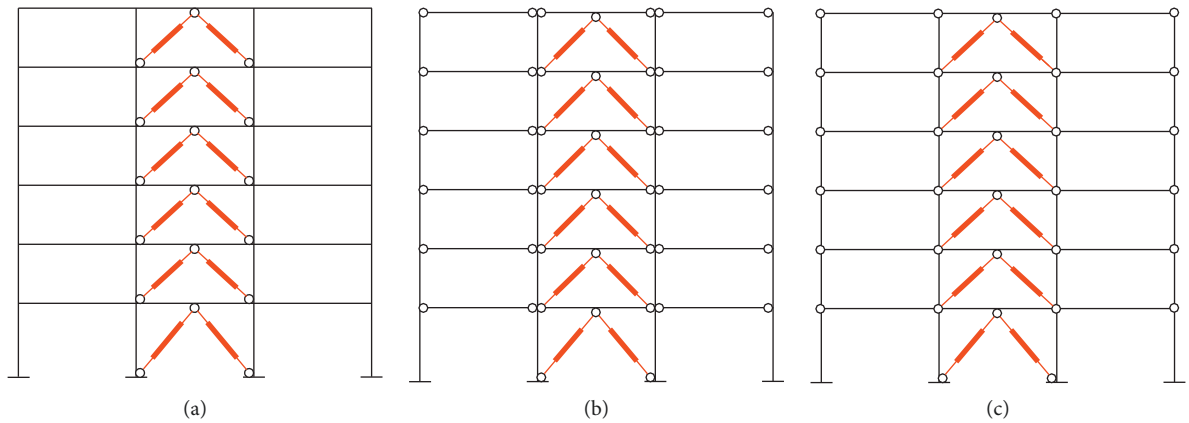

Figure 6: Three types of structures: (a) BRBF-RBC; (b) BRBF-PBC; (c) BRBT.

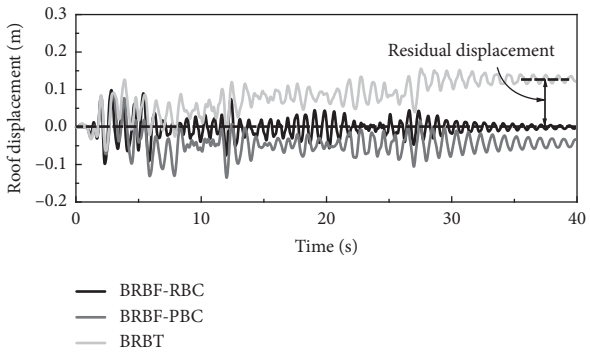

Figure 7: Comparison of the roof displacement time-history responses.

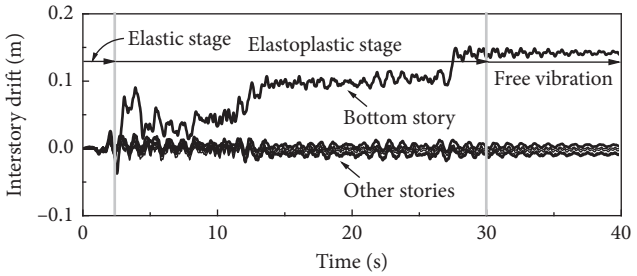

Figure 8: Interstory drift time-history response.

stories generally underwent synchronous development before the initial yield of the BRBs. Once the BRBs yielded, the deformation was concentrated in the bottom story due to the DCE. The displacement response of the structure was almost completely provided by the bottom story deformation, while the interstory displacements of other stories were small. The bottom story (soft story) played a certain role in the vibration isolation, preventing the seismic energy from reaching the upper story. This centralized damage pattern could cause interlayer collapse, which is worth noting in the design of BRBFs.

Figure 9 shows the relationship between the DCF and the roof displacement of three different structures under a NPA based on an inverted triangle lateral force. The damage concentration of the BRBT is the most obvious. When the roof displacement of the structure reaches 1.0 m, the BRBT DCF tends toward its maximum value of 6, which indicates that the structural damage is completely concentrated in the soft story. The BRB at the bottom story yields first; thus, the interstory stiffness is approximately zero, and the DCF increases linearly. The results show that a second structural stiffness (MF stiffness) is a necessary condition for avoiding a weak story.

Although a large residual displacement is observed in the BRBF-PBC after the earthquake (See Figure 7), the BRBF-PBC shows a small DCF during the entire NPA process, indicating that the continuous and uniform column can play a role similar to that of a rocking system. The lateral stiffness provided by the MF in the BRBF-RBC is larger than that provided by the column in the BRBF-PBC, and the DCF of the BRBF-RBC is larger. The rigid and pin beam-to-column connections are essentially different in terms of the beam-column flexural strength ratio. The beam-column flexural strength ratio in the MF with pin beam-to-column connections can be regarded as zero. The results show that the MF beam-column flexural strength ratio significantly affects the structural DCE and that a "strong column-weak beam" is also a necessary condition for avoiding a soft story.

4. Structural Models for Parametric Analysis

4.1. Benchmark Building. The benchmark building is designed as a dual system of BRBs and an MRF following the criteria developed in the Chinese seismic code [24]. The building is assumed to be located in an area with Site Classification III and design ground Group 1, classified as a zone of Intensity 8, with a basic design peak ground acceleration (PGA) of 0.4 g. Figure 10 presents the structural layouts of the BRBF buildings. The structural plane shown in Figure 10(a) is a rectangle of 24 m by 50.4 m composed of 7 transverse axes and 4 longitudinal axes. The column spacing is 8.4 m, and the dead load and live load are 6.0 kN/m^2 and 2.0 kN/m^2, respectively. The same steel grade, structural span, and story height with the example shown in Figure 3 are used in this benchmark building.

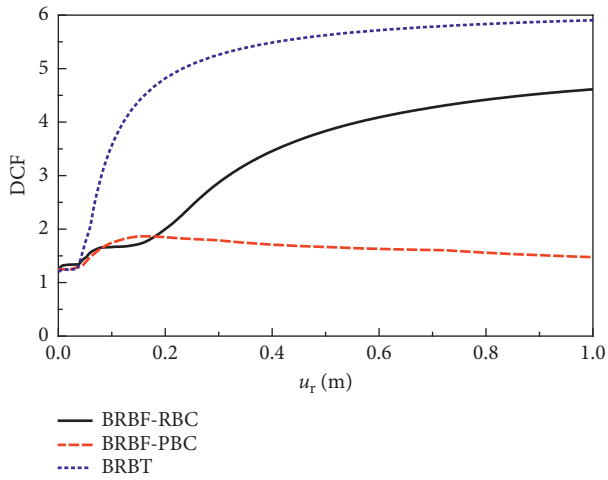

Figure 9: DCF responses of three structures with different beam-to-column connections.

In this article, only the transverse seismic design is considered. The transverse earthquake resisting system comprises two BRBFs on outside of the 1st and 7th axes. The pinned columns on the 2nd to 6th axes bear only gravity, and all the columns work together through the rigid floor. Figure 10(b) shows the vertical layout of the transverse frame; the left side span is arranged with inverted V braces.

For simplicity and due to symmetry, only one transverse frame with half of the structural weight is investigated in this research, and only half of the live load is considered when calculating the seismic action. As a result, the equivalent values of the dead load and the live load on the beams of each story are 25.2 kN/m and 8.4 kN/m, respectively. The equivalent mass of each story is 423360 kg. In the preliminary design, the beam-column sizes are determined to be the same as those of the frame shown in Figure 3, and the area of all BRBs is 4000 mm^2.

The structures are examined under a small earthquake (63% probability of exceedance in 50 years) based on the Chinese seismic code [24]. Figure 11 shows the design and verification process. The mode-superposition response spectrum method is used to determine the equivalent earthquake force. The seismic actions, dead loads, and live loads are considered in the load effect combination. The design rule of the structural members is that the force resistance of each member should exceed the design force. In other words, the ratio of the design force to the force resistance (stress ratio) should be less than 1. The BRBs are considered as axial tensile and compressive members, while the beams and the columns in the frame are considered as flexural members and compression-flexural members, respectively. The interstory shear force of the MF, calculated according to the relative stiffness, should be adjusted to the minimum value between 25% of the structural total shear at the bottom story and 1.8 times the maximum interstory shear force of the MF, which is used to verify the bearing capacity of the MF (25%-1.8 rule). The interstory drift ratio is 1/456, and the stress ratios of the structural members (considering the 25%-1.8 rule) that satisfy the code requirements are shown in Table 1. A design process for a BRBF related to the European seismic code can be found in Vigh et al. [34].

4.2. Numerical Models. Figure 12 schematically shows the finite element model for half of the benchmark building, which is similar to the finite element model mentioned in Section 3.1. The mass of each story is concentrated at the node of the right gravity-resisting system.

Table 2 presents a set of 22 ground motions recommended for structural seismic performance analysis (Qu 2010 [35]). According to the Chinese code and the seismic design conditions of the design example above, all the peak accelerations of the motions are set to 4 m/s^2 for the RHA of the BRBFs. The original PGA and the scale factor of the design PGA (4 m/s^2) are listed in Table 2. Figure 13 compares the design spectrum with the spectra of actual waves, including the acceleration spectra and displacement spectra, and shows that the average spectrum of the actual waves is very similar to the design spectrum.

4.3. Stiffness Distribution Parameters. The nature of a structural damage mechanism is the size and development tendency of the internal force and deformation, which are mainly affected by the distribution of seismic force and structural stiffness. To provide a reference for BRBF design, this paper evaluates the effects of the two parameters characterizing the structural stiffness distributions between the BRB and the frame (horizontal direction) and that among the different stories (vertical direction) on the DCE and seismic structural responses.

(1) A consistent interstory stiffness of the BRB relative to the frame at each story is difficult to achieve, although the structural story height and component sizes do not change. The fundamental period ratio of the truss formed by the BRBs and their adjacent beam-columns to the MF are used to approximately define the BRB-frame stiffness ratio γ_1, as shown in equation (4). T_{BRB} and T_{MF} are the fundamental periods of the truss and the MF, respectively.

$$\gamma_1 = \frac{T_{\mathrm{MF}}}{T_{\mathrm{BRB}}}. \tag{4}$$

(2) The core of the BRBs is assumed to be made of steel with the same elastic modulus. The BRB stiffness ratio between adjacent stories γ_2 is defined in equation (5), where A^i_{BRB} is the core area of the BRBs at the ith story and N is the number of stories.

$$\gamma_2 = \frac{A^{i-1}_{\mathrm{BRB}}}{A^i_{\mathrm{BRB}}}, \quad i = 2, 3, \ldots, N. \tag{5}$$

In summary, γ_1 mainly measures the stiffness ratio of the BRB to the MF. When the stiffness provided by the BRBs is larger, γ_1 is larger, implying that the BRB is the main lateral resistance system in BRBFs. γ_2 can reflect the distribution of the structural stiffness in the vertical direction. When γ_2 is

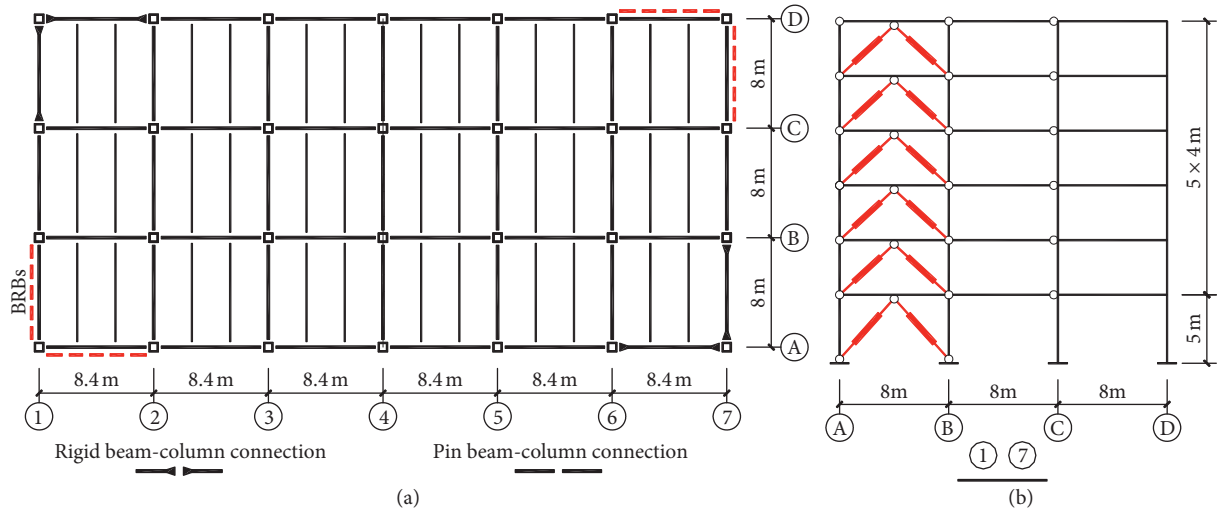

Figure 10: Structural layout of benchmark building: (a) plan layout and (b) vertical layout on the 4th and 7th axes.

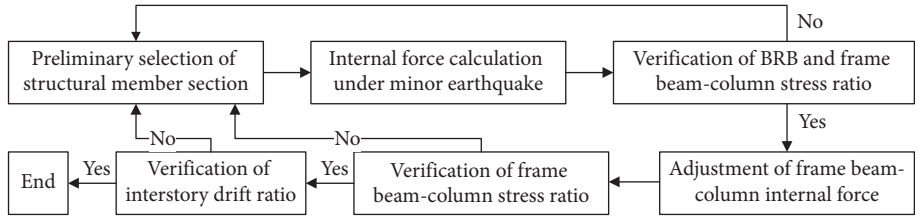

Figure 11: Flow chart of BRBF design.

Table 1: Verification results for the stress ratio.

Story	Unadjusted			Adjusted	
	BRB	Beam	Column	Beam	Column
1	0.934	0.226	0.247	0.376	0.411
2	0.811	0.188	0.089	0.861	0.408
3	0.696	0.183	0.083	0.643	0.292
4	0.591	0.169	0.077	0.641	0.292
5	0.463	0.139	0.070	0.582	0.293
6	0.275	0.091	0.057	0.511	0.320

close to 1, the structural stiffness is distributed evenly along the height.

4.4. Parametric Models. Based on the benchmark model shown in Figure 12, keeping the MF constant, the parametric models and their periods are shown in Figure 14, where 21 parametric models are built for each parameter. As shown in Figure 14(a), different γ_1 values are generated based on the mean change in the area of the BRBs from 0 to 8000 mm^2. In Figure 14(b), the area of the BRBs at the bottom story is 4000 mm^2, and different γ_2 values are generated based on the mean change in the area of the BRBs at the upper stories.

5. Parametric Analysis Results

5.1. BRB-Frame Stiffness Ratio, γ_1. NPAs of the parametric models are conducted for various γ_1 values. Figure 15 shows the curves of the structural base force relative to the roof displacement. The BRB postyield stiffness is assumed to be approximately zero. As γ_1 increases, the structural initial stiffness increases because of the increased BRB area, while the structural postyield stiffness remains unchanged because of the constant MF stiffness. Therefore, the structural postyield stiffness ratio decreases as γ_1 increases, implying that the BRBF stiffness decreases significantly after the BRBs yield when the structure uses a BRB as the main seismic resistance system. γ_1 mainly measures the ratio of the postyield stiffness to the initial stiffness of the BRBFs.

Figure 16 shows curves of the damage performance indices presented in Section 2.2 and the BRB-frame stiffness ratio. u_r and θ_{max} decrease as γ_1 increases, which indicates that an additional BRB can provide lateral stiffness and energy dissipation for a structure, thus reducing the displacement response of the structure. u_{rr} and θ_{rmax} are not significantly reduced when γ_1 increases, which mainly occurs because the structure postyield stiffness ratio decreases (See Figure 15), although the displacement responses decrease as γ_1 increases. Therefore, if the displacement responses of two structures are the same, the one with a larger γ_1 undergoes a larger residual displacement. The DCF and RDCF increase as γ_1 increases. When γ_1 is larger, the abrupt change in the interstory stiffness between various stories after the BRBs at one story yield is greater. Thus, a more obvious DCE occurs. The u_r and θ_{max} of the MRF ($\gamma_1 = 0.00$) are approximately 3.0% and 0.5%, respectively, and the DCF and RDCF values are 1.18 and

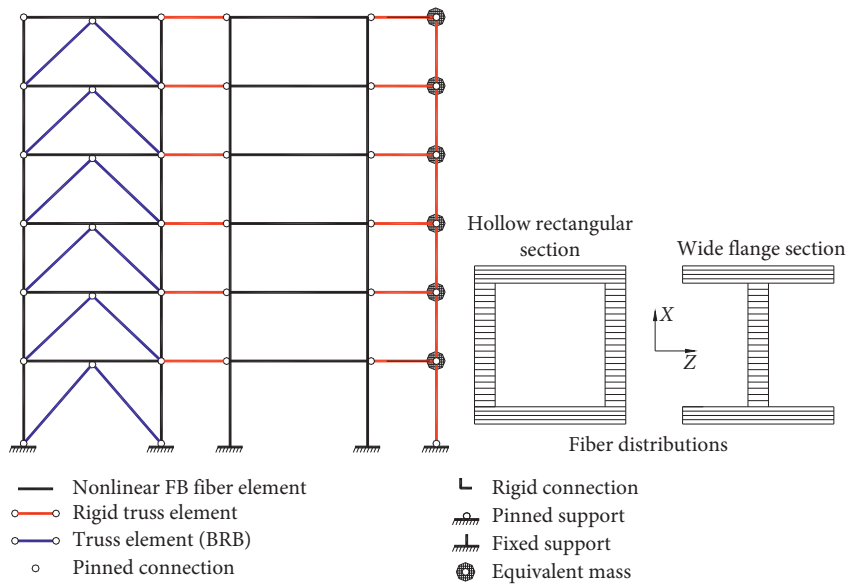

Figure 12: Sketch of OpenSees models.

Table 2: Earthquake waves used in the examples.

Id	Earthquake	Year	[a]M	Duration/s	[b]FD/km	[c]PGA/(m/s^2)	[d]SF
1	Friuli, Italy 01	1976	6.50	36.345	14.97	2.93	1.36
2	Imperial Val.-06	1979	6.53	99.920	22.03	3.44	1.16
3	Imperial Val.-06	1979	6.53	39.330	12.69	2.00	2.00
4	Superst. Hills-02	1987	6.54	44.000	23.85	1.82	2.20
5	Loma Prieta	1989	6.93	39.945	12.23	3.60	1.11
6	Loma Prieta	1989	6.93	39.640	24.52	2.07	1.94
7	Loma Prieta	1989	6.93	59.955	27.67	3.63	1.10
8	Landers	1992	7.28	27.965	19.74	3.04	1.31
9	Landers	1992	7.28	44.000	11.03	2.78	1.44
10	Landers	1992	7.28	44.000	23.62	1.65	2.42
11	Northridge-01	1994	6.69	19.990	11.39	4.72	0.85
12	Northridge-01	1994	6.69	40.000	20.10	5.57	0.72
13	Northridge-01	1994	6.69	40.000	17.28	7.38	0.54
14	Kobe, Japan	1995	6.90	40.960	22.50	3.38	1.18
15	Kobe, Japan	1995	6.90	40.960	19.14	2.38	1.68
16	Duzce, Turkey	1999	7.14	55.900	12.02	8.06	0.50
17	Chichi, Taiwan-05	1999	7.62	90.000	28.05	1.97	2.03
18	Chichi, Taiwan-05	1999	7.62	90.000	19.02	2.50	1.60
19	Chichi, Taiwan-05	1999	7.62	90.000	45.15	3.35	1.20
20	Wenchuan	2008	8.00	250.005	18.76	4.59	0.87
21	Wenchuan	2008	8.00	250.005	24.27	2.79	1.43
22	Wenchuan	2008	8.00	309.000	15.66	3.23	1.24

[a]Magnitude; [b]fault distance; [c]original earthquake ground motion records; [d]scale factor (SF) of 4 m/s^2 to the original PGA.

1.23, respectively. Therefore, although the lateral stiffness of the MRF is small and the seismic damage is large, the damage is relatively homogeneous. When a BRB is designed as the main lateral force resistance system, the structural DCE is obvious.

5.2. BRB Stiffness Ratio between Stories, γ_2. Figure 17 shows the relationship between the damage performance index and the BRB area ratio γ_2 along the structural height. The u_r response of the structure decreases as γ_2 increases because the natural period of the structure decreases (See Figure 14(b)). u_{rr} and θ_{rmax} undergo no obvious change as γ_2 increases. The θ_{max} response first decreases and then increases as γ_2 increases. The minimum value appears when γ_2 is approximately 0.8. In addition, when γ_2 is greater than 0.8, the DCF and RDCF of the structure increase significantly as γ_2 increases; that is, when the upper floor is larger than the BRB area of the lower floor, the DCE of the structure is obvious. Therefore, the BRB should be continuously arranged along the floor in the frame, and the area can be gradually reduced along the height. The arrangement corresponding to a γ_2 value of 0.8 can make the structural interstory drift response small and uniform.

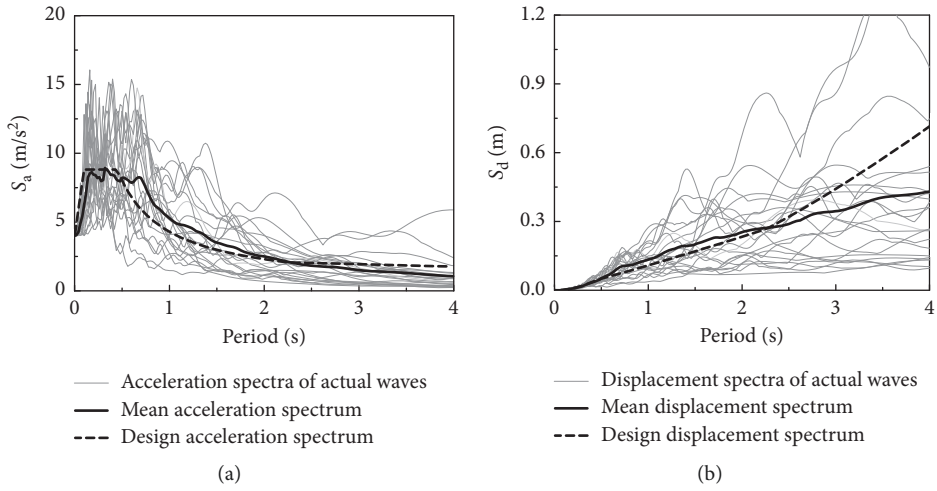

Figure 13: Design spectrum and spectra of actual waves: (a) acceleration spectra; (b) displacement spectra.

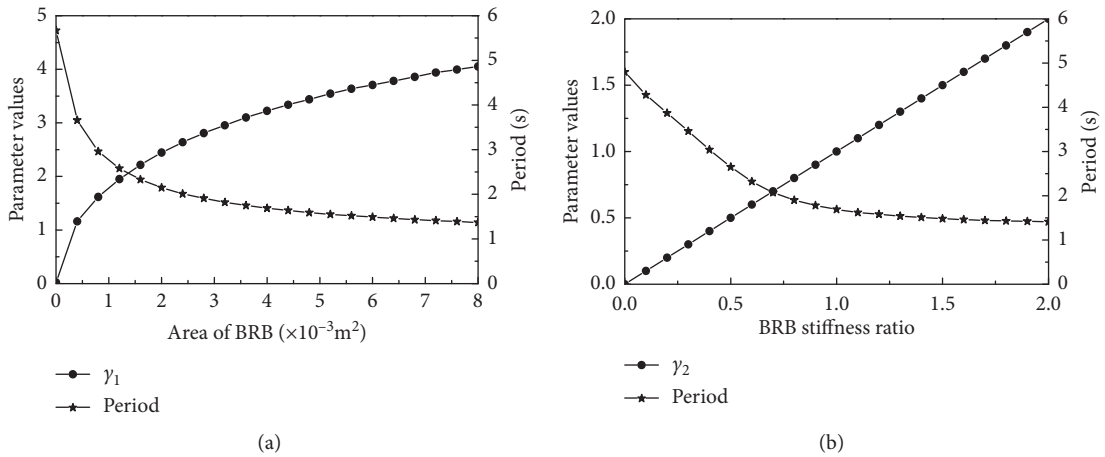

Figure 14: Parametric models and their periods.

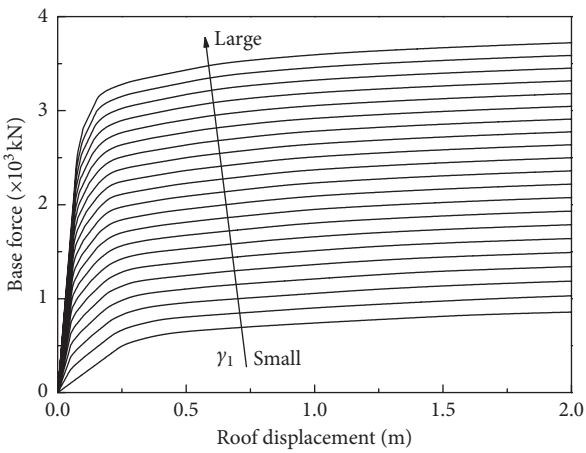

Figure 15: Curves of structural base force relative to the roof displacement for various γ_1 values.

Figure 18 shows the plastic rotation θ_p at the ends of the frame beams and columns for different γ_2 values. The θ_p results are the average values of 22 ground motions. Figures 18(b) and 18(c) show that when γ_2 is close to or equal to 1, the plastic rotation of the frame is not more than 0.01 and a plastic hinge with an angle between 0.005 and 0.01 mainly appears at the beam end and the column base. In Figure 18(a), when the upper BRB area is small (γ_2 is small), the value of θ_p at the end of the frame beam is greater than 0.01 and that of the frame column is less than 0.005. In Figure 18(d), γ_2 is large, that is, the BRB area of the lower floor is small. Only the frame of the bottom story has the hinge, while the upper story is in the elastic state, and the plastic rotation of the bottom column is greater than 0.01. According to the figure, as γ_2 increases, the number and value of plastic hinges on the frame beam gradually decrease, the number of plastic hinges on the frame column is reduced, and the size of the bottom column plastic hinge angle increases. Thus, the damage is completely concentrated at the bottom story of the structure. Therefore, the value of γ_2 affects the damage mechanism of the frame. The BRB area should be gradually reduced from the bottom to the top to avoid the story yielding mechanism, with the upper story being hindered from entering the yield state.

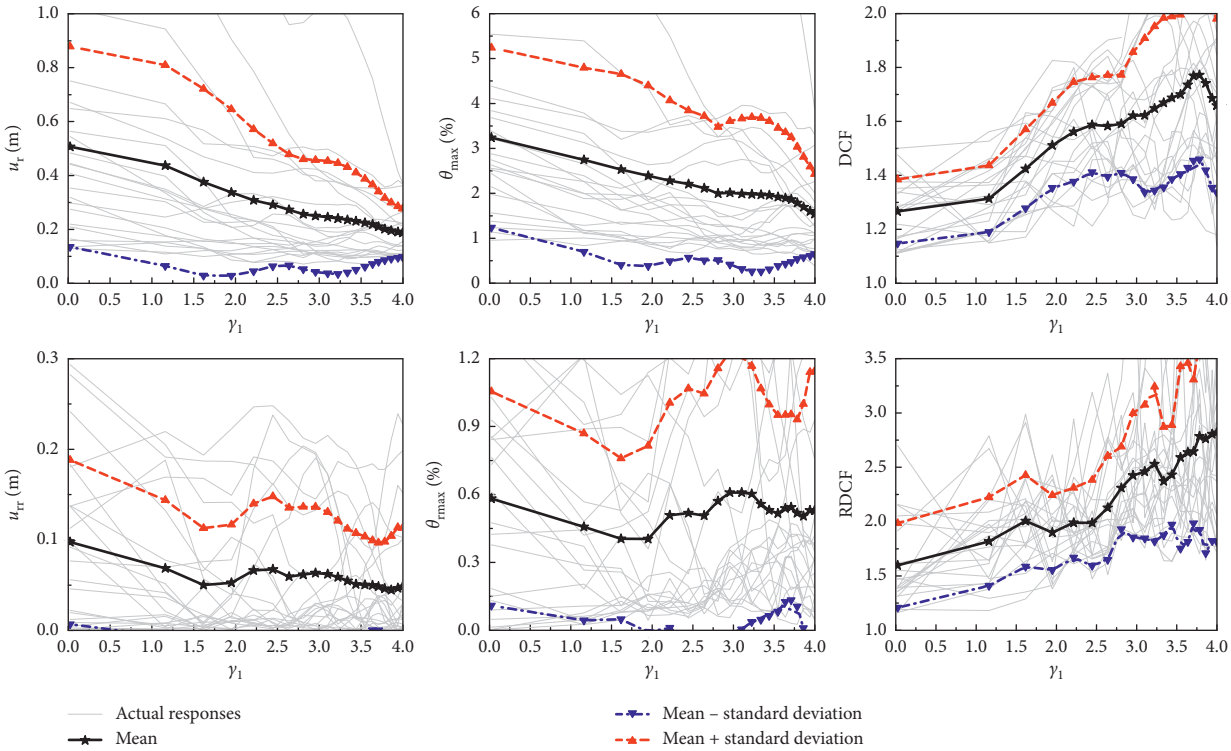

Figure 16: Parametric analysis results for BRB-frame stiffness ratio.

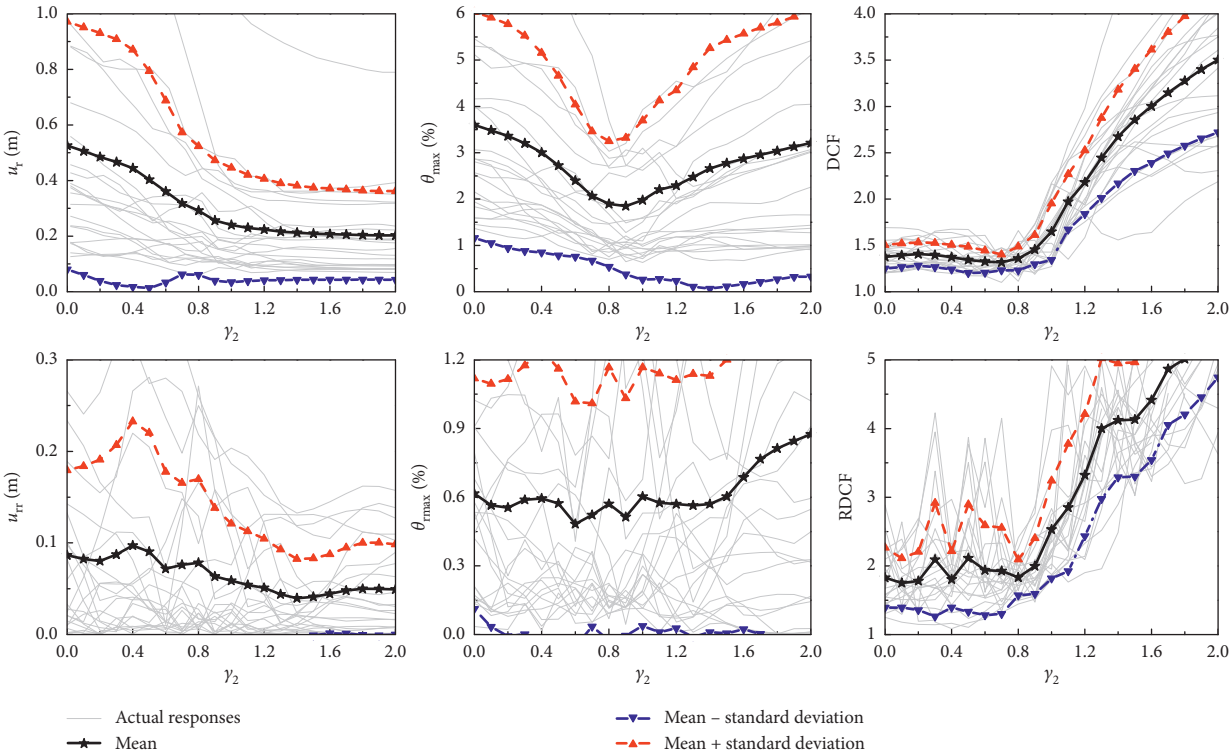

Figure 17: Parametric analysis results for BRB stiffness ratio between stories.

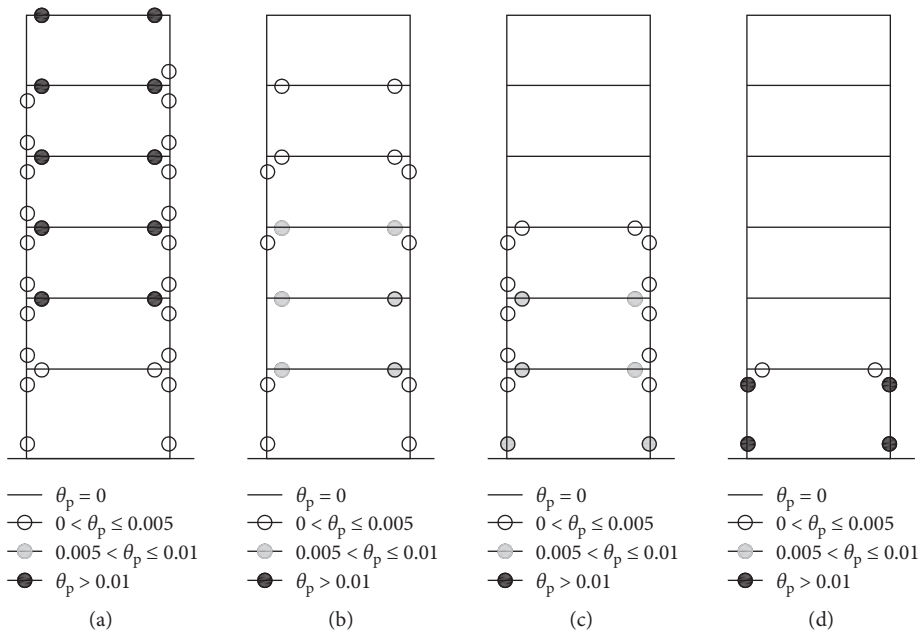

Figure 18: Plastic rotation of the frame beams and columns. (a) $\gamma_2 = 0.10$, (b) $\gamma_2 = 0.80$, (c) $\gamma_2 = 1.00$, (d) $\gamma_2 = 0.10$.

6. Correlation between Performance Indices

This section examines whether there is a correlation between performance indices. If two performance indices have a completely linear correlation, then the value of one index can be obtained from that of the other based on the correlation. Thus, only one of the two performance indices would have to be analyzed in the seismic evaluation of a BRBF. All weak correlation indices should be considered to accurately evaluate the seismic performance of a structure. Due to the randomness of the ground motions, even if the peak acceleration of each ground motion is set to the same value, the performance index response of the structure under this set of ground motions will be different. Therefore, the correlation coefficient of the two indices is calculated using equation (6) for the analysis of the six damage performance indices presented in Section 2.2.

$$CC = \frac{\sum_{i=1}^{n} (x_i - \overline{x})(y_i - \overline{y})}{\sqrt{\sum_{i=1}^{n} (x_i - \overline{x})^2 \sum_{i=1}^{n} (y_i - \overline{y})^2}}, \quad (6)$$

where CC is the index correlation coefficient, n is the number of ground motions, x_i and y_i are the responses of an index pair under the i-th ground motion, and $\overline{x}$ and $\overline{y}$ are the average responses to an index pair for all ground motions.

Figure 19 shows the average of the correlation coefficients for each performance index. An absolute value of CC that is greater than or equal to 0.8 denotes a high correlation, a value in the range of [0.5, 0.8) denotes a moderate correlation, a value in the range [0.3, 0.5) implies a low correlation, and a value of less than 0.3 indicates a very weak correlation.

The correlations between u_r and θ_{max} and between u_{rr} and θ_{rmax} are high. This conclusion is consistent with the results of Ruiz-Garcia [36]. u_r is moderately correlated with u_{rr}, θ_{max}, and θ_{rmax}. The DCF is moderately correlated to u_r and θ_{rmax}, while the other performance indicators have a low correlation with the DCF. The RDCF has a low correlation with the DCF, and the other performance indices are weakly correlated with the RDCF. In conclusion, the correlation between the displacement response and the residual displacement response is not high. Therefore, u_r can be a good measure of the magnitude of θ_{max}, while the displacement (angle) is not related to the residual displacement (angle). The use of the roof displacement or interstory drift ratio as the only index of the seismic performance for structures requiring damage consideration and postearthquake repair functions, such as BRBFs, is thus not appropriate. Instead, the use of the displacement and residual displacements or DCF as two-dimensional control parameters for the seismic performance analysis and design of BRBFs is recommended.

7. Summary and Conclusions

The postyield stiffness of a BRB is low, and the BRBs at all stories cannot simultaneously enter the yield stage during an earthquake. The yield of the BRBs at one story or certain stories will cause a story stiffness mutation when a structure is in the elastic-plastic stage. Therefore, BRBFs equipped with BRBs as the main lateral resistance system are prone to lateral deformations and damage concentration at certain stories, leading to a larger residual deformation in the structures and inducing an obvious DCE. Two comparisons of the DCE for different structural types and different beam-to-column connections of the MF are performed, and the influence of the BRB-frame stiffness ratio and BRB stiffness ratio between stories on the structural DCEs are investigated for multistory BRBFs. The conclusions are as follows:

(1) The added BRBs are effective at dissipating energy and controlling interstory drift, thus improving the

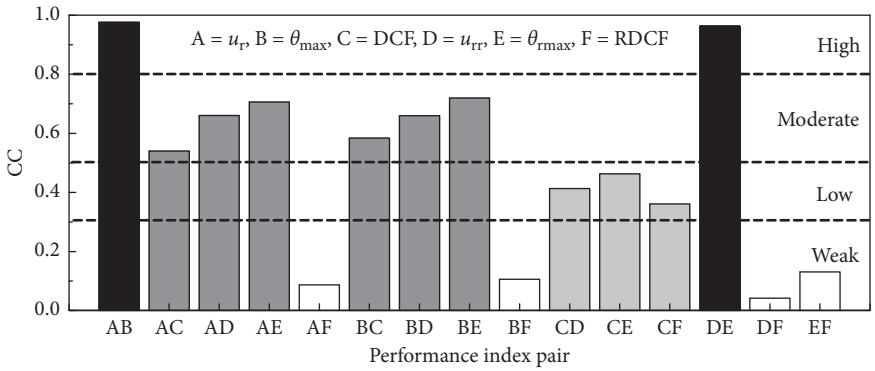

Figure 19: Average values of correlation coefficients between indices.

seismic performance of the original MRF. However, the BRBs have a low postyield stiffness and the BRBFs have a more serious interstory DCE than the traditional MRF or CBF.

(2) It is necessary to ensure that the MF in BRBFs has a certain stiffness. The second stiffness of the structure can cause the majority of the BRBs to yield and can reduce the DCE and residual deformation of the structure. The MF beam-column flexural strength ratio significantly affects the structural DCE, and a "strong column-weak beam" is a necessary condition for avoiding a weak story.

(3) The added BRBs can provide the initial stiffness and energy dissipation for the MRF, thus reducing the structural displacement response under earthquakes. However, the structural DCF increases as the BRB-frame stiffness ratio increases. When a BRB is the main lateral force resistance system in the BRBF, the structural DCE is obvious.

(4) The BRB stiffness ratio between stories affects the damage mechanism of the frame. The BRB layout in the frame for a BRB area ratio of 0.8 between stories from the bottom to the top can make the interstory drift ratio relatively small and more uniform.

(5) The correlations between (residual) roof displacement and (residual) interstory drift ratio are high. However, the correlations between roof displacement (interstory drift ratio) and residual roof displacement (interstory drift ratio) are low, and the correlation coefficients between the DCF and other performance indices are weak.

In conclusion, the use of the displacement and residual displacement (or DCF) as the two dual control indices for BRBF evaluation and design is recommended. These conclusions may be limited to numerical models used in the paper and should be further validated.

Symbols

θ_{max}: maximum interstory drift ratio
θ_{ave}: average interstory drift ratio
u_r: roof displacement
DCF: drift concentration factor
DCF_2: DCF of two-story structures
h: story height
F: lateral force at the first floor
k_1: first story stiffness
k_2: second story stiffness
θ_{rmax}: residual drift ratio
u_{rr}: residual roof displacement
RDCF: residual drift concentration factor
E: elastic modulus
PGA: peak ground acceleration
γ_1: BRB-frame stiffness ratio
γ_2: BRB stiffness ratio between adjacent stories
T_{BRB}: fundamental period of BRB truss
T_{MF}: fundamental period of main frame
A_{BRB}^i: core area of BRBs at i-th story
N: number of stories
θ_p: plastic rotation of the frame beams and columns
CC: index correlation coefficient
n: number of ground motions
x_i and y_i: responses of an index pair under the i-th ground motion
$\overline{x}$ and $\overline{y}$: average responses to an index pair for all ground motions.

Data Availability

The authors declare that all data supporting the findings of this study are available within the article.

Conflicts of Interest

The authors declare that there are no conflicts of interest regarding the publication of this paper.

Acknowledgments

The research described in this paper was sponsored by the National Natural Science Foundation of China (51708166) and a project funded by China Postdoctoral Science Foundation (2018M630706). This support is gratefully acknowledged.

References

[1] C. M. Uang, M. Nakashima, and K. C. Tsai, "Research and application of buckling-restrained braced frames," *International Journal of Steel Structures*, vol. 4, no. 4, pp. 301–313, 2004.

[2] M. Yamaguchi, S. Yamada, Y. Matsumoto et al., "Full-scale shaking table test of damage tolerant structure with a buckling resistant brace," *Journal of Structural and Construction Engineering (Transactions of AIJ)*, vol. 67, no. 558, pp. 189–196, 2002.

[3] G. R. Kumar, S. R. S. Kumar, and V. Kalyanaraman, "Behaviour of frames with non-buckling bracings under earthquake loading," *Journal of Constructional Steel Research*, vol. 63, no. 2, pp. 254–262, 2007.

[4] B. Asgarian and N. Amirhesari, "A comparison of dynamic nonlinear behavior of ordinary and buckling restrained braced frames subjected to strong ground motion," *The Structural Design of Tall and Special Buildings*, vol. 17, no. 2, pp. 367–386, 2008.

[5] Y. Ding, R. Zheng, and W. Zhang, "Tests of chevron panel buckling-restrained braced steel frames," *Journal of Constructional Steel Research*, vol. 143, pp. 233–249, 2018.

[6] P. Jones and F. Zareian, "Seismic response of a 40-storey buckling-restrained braced frame designed for the Los Angeles region," *The Structural Design of Tall and Special Buildings*, vol. 22, no. 3, pp. 291–299, 2013.

[7] J. W. Lai, C. H. Chen, and S. A. Mahin, "Experimental and analytical performance of concentrically braced steel frames," in *Proceedings of Structures Congress*, ASCE, Reston, VA, USA, 2010.

[8] C. H. Chen and S. A. Mahin, "Performance-based seismic demand assessment of concentrically braced steel frame buildings," Pacific Earthquake Engineering Research Center, University of California, Berkeley, CA, USA, PEER Report 2012/103, 2012.

[9] B. G. Simpson and S. A. Mahin, "Experimental and numerical evaluation of older chevron concentrically braced frames with hollow and concrete-filled braces," *Journal of Structural Engineering*, vol. 144, no. 3, article 04018007, 2018.

[10] R. Sabelli, S. Mahin, and C. Chang, "Seismic demands on steel braced frame buildings with buckling-restrained braces," *Engineering Structures*, vol. 25, no. 5, pp. 655–666, 2003.

[11] S. Zaruma and L. A. Fahnestock, "Assessment of design parameters influencing seismic collapse performance of buckling-restrained braced frames," *Soil Dynamics and Earthquake Engineering*, vol. 113, pp. 35–46, 2018.

[12] L. A. Fahnestock, J. M. Ricles, and R. Sause, "Experimental evaluation of a large-scale buckling-restrained braced frame," *Journal of Structural Engineering*, vol. 133, no. 9, pp. 1205–1214, 2007.

[13] J. Erochko, C. Christopoulos, R. Tremblay, and H. Choi, "Residual drift response of SMRFs and BRB frames in steel buildings designed according to ASCE 7-05," *Journal of Structural Engineering*, vol. 137, no. 5, pp. 589–599, 2011.

[14] S. Kiggins and C.-M. Uang, "Reducing residual drift of buckling-restrained braced frames as a dual system," *Engineering Structures*, vol. 28, no. 11, pp. 1525–1532, 2006.

[15] C. Ariyaratana and L. A. Fahnestock, "Evaluation of buckling-restrained braced frame seismic performance considering reserve strength," *Engineering Structures*, vol. 33, no. 1, pp. 77–89, 2011.

[16] A. F. Ghowsi and D. R. Sahoo, "Seismic performance of buckling-restrained braced frames with varying beam-column connections," *International Journal of Steel Structures*, vol. 13, no. 4, pp. 607–621, 2013.

[17] D. R. Sahoo and S. H. Chao, "Stiffness-based design for mitigation of residual displacements of buckling-restrained braced frames," *Journal of Structural Engineering*, vol. 141, no. 9, article 04014229, 2014.

[18] D. J. Miller, L. A. Fahnestock, and M. R. Eatherton, "Development and experimental validation of a nickel-titanium shape memory alloy self-centering buckling-restrained brace," *Engineering Structures*, vol. 40, pp. 288–298, 2012.

[19] Z. Zhou, Q. Xie, X. Lei et al., "Experimental investigation of the hysteretic performance of dual-tube self-centering buckling-restrained braces with composite tendons," *Journal of Composites for Construction*, vol. 19, no. 6, article 04015011, 2015.

[20] R. Tremblay, "Achieving a stable inelastic seismic response for multi-story concentrically braced steel frames," *Engineering Journal*, vol. 40, no. 2, pp. 111–129, 2003.

[21] B. G. Simpson and S. A. Mahin, "Experimental and numerical investigation of strongback braced frame system to mitigate weak story behavior," *Journal of Structural Engineering*, vol. 144, no. 2, article 04017211, 2017.

[22] T. Takeuchi, X. Chen, and R. Matsui, "Seismic performance of controlled spine frames with energy-dissipating members," *Journal of Constructional Steel Research*, vol. 114, pp. 51–65, 2015.

[23] L. Chen, R. Tremblay, and L. Tirca, "Practical seismic design procedure for steel braced frames with segmental elastic spines," *Journal of Constructional Steel Research*, vol. 153, pp. 395–415, 2019.

[24] MOHURD, *Code for Seismic Design of Buildings, GB 50011-2010*, Ministry of Housing and Urban-Rural Development of the People's Republic of China (MOHURD), Beijing, China, 2010, in Chinese.

[25] G. A. MacRae, Y. Kimura, and C. Roeder, "Effect of column stiffness on braced frame seismic behavior," *Journal of Structural Engineering*, vol. 130, no. 3, pp. 381–391, 2004.

[26] J. McCormick, H. Aburano, M. Ikenaga et al., "Permissible residual deformation levels for building structures considering both safety and human elements," in *Proceeding of 14th World Conference Earthquake Engineering*, Beijing, China, October 2008.

[27] Open System for Earthquake Engineering Simulation (OpenSees), *Pacific Earthquake Engineering Research Center*, University of California, Berkeley, CA, USA, 2007, http://opensees.berkeley.edu.

[28] P. Uriz and S. A. Mahin, "Toward earthquake-resistant design of concentrically braced steel-frame structures," Pacific Earthquake Engineering Research Center, University of California, Berkeley, CA, USA, PEER Report 2008/08, 2008.

[29] B. Qu, F. Sanchez-Zamora, and M. Pollino, "Mitigation of inter-story drift concentration in multi-story steel concentrically braced frames through implementation of rocking cores," *Engineering Structures*, vol. 70, pp. 208–217, 2014.

[30] A. K. Chopra, *Dynamics of Structures: Theory and Applications to Earthquake Engineering*, Pearson Education Inc, Englewood Cliffs, NJ, USA, 2nd edition, 2001.

[31] M. D'Aniello, S. Costanzo, and R. Landolfo, "The influence of beam stiffness on seismic response of chevron concentric bracings," *Journal of Constructional Steel Research*, vol. 112, pp. 305–324.

[32] S. Costanzo, M. D'Aniello, and R. Landolfo, "The influence of moment resisting beam-to-column connections on seismic behavior of chevron concentrically braced frames," *Soil*

Dynamics and Earthquake Engineering, vol. 113, pp. 136–147, 2018.

[33] V. R. Wigle and L. A. Fahnestock, "Buckling-restrained braced frame connection performance," *Journal of Constructional Steel Research*, vol. 66, no. 1, pp. 65–74, 2010.

[34] L. G. Vigh, Á. Zsarnóczay, and T. Balogh, "Eurocode conforming design of BRBF - Part I: Proposal for codification," *Journal of Constructional Steel Research*, vol. 135, pp. 265–276, 2017.

[35] Z. Qu, *Study on seismic damage mechanism control and design of rocking wall-frame structures*, Ph.D. thesis, Department of Civil Engineering, Tsinghua University, Beijing, China, 2010, in Chinese.

[36] J. Ruiz-Garcia, "On the influence of strong-ground motion duration on residual displacement demands," *Earthquakes and Structures*, vol. 1, no. 4, pp. 327–344, 2010.